Journal of Biomedical Materials Research Part B: Applied Biomaterials

Amoxicillin-loaded electrospun nanocomposite membranes for dental applications

Journal:	*Journal of Biomedical Materials Research: Part B - Applied Biomaterials*
Manuscript ID	JBMR-B-15-0676.R2
Wiley - Manuscript type:	Original Research Report
Date Submitted by the Author:	15-Jan-2016
Complete List of Authors:	Furtos, Gabriel; Institute of Research in Chemistry Rivero, Guadalupe; INTEMA, Biomedical Polymers Division Rapuntean, Sorin ; University of Agricultural Sciences and Veterinary Medicine Abraham, Gustavo; INTEMA, Biomedical Polymers Division
Keywords:	electrospun scaffolds, antibiotic delivery, mineralization, antibacterial activity

Amoxicillin-loaded electrospun nanocomposite membranes for dental applications

Gabriel Furtos[1,§], Guadalupe Rivero[2,§], Sorin Rapuntean[3], Gustavo A. Abraham[2]

[1]*Babes-Bolyai University-Raluca Ripan, Institute of Research in Chemistry, Cluj-Napoca, Romania. gfurtos@yahoo.co.uk*

[2]*Research Institute for Materials Science and Technology (INTEMA), Av. Juan B. Justo 4302, B7608FDQ, Mar del Plata, Argentina. gabraham@fi.mdp.edu.ar, grivero@fi.mdp.edu.ar.*

[3]*University of Agricultural Sciences and Veterinary Medicine, Cluj-Napoca, Romania, sorin.rapuntean@gmail.com*

[§]*These authors equally contributed to the work.*

Abstract

Electrospun nanocomposite matrices based on poly(ε-caprolactone) (PCL), nano-hydroxyapatite (nHAp) and amoxicillin (AMX) were designed and investigated for dental applications. nHAp provides good biocompatibility, bioactivity, osteoconductivity and osteoinductivity properties, and AMX, as antibiotic model, controls and/or reduces bacterial contamination of periodontal defects while enhancing tissue regeneration. A series of polymeric nanocomposites was obtained by varying both the antibiotic and nHAp contents. Fibrous membranes of different compositions were obtained by electrospinning technique, and morphological, thermal, mechanical and surface properties were characterized. The incorporation of AMX seemed to alter the

nHAp distribution within the microfibrous matrix. The interaction between AMX and nHAp affected the mechanical performance and modulated the antibiotic release behavior. AMX release profiles presented a burst release that depended on nHAp content, followed by a slow release stage where the drug content (85-100%) was released in 3 weeks. The antimicrobial activity of the AMX-loaded membranes was tested with four bacterial strains depended on both the drug and nHAp contents. Extensive mineralization in simulated body fluid (SBF) was evidenced by SEM/EDX analysis after 21 days. The studied electrospun nanocomposite amoxicillin-loaded membranes could be a promising fibrous-based antibiotic carrier system for dental and tissue engineering applications.

Keywords: electrospun scaffolds, antibiotic delivery, mineralization, antibacterial activity

INTRODUCTION

Electrospinning is a fascinating and powerful processing technique with huge potential in many attractive and cutting-edge research fields.[1] This electrohydrodynamic technique allows the production of non-woven micro/nanofibrous structures, including natural or synthetic polymers, ceramics, metals and nanocomposites, with a wide range of morphologies and functionalities. The resulting highly porous structures are ideal for many biomedical applications, in particular for the production of tissue-engineered constructs and therapeutic delivery systems.[2-4]

In guided tissue/bone regeneration (GTR/GBR), a dental surgical procedure for promoting new bone formation, a barrier membrane is used to block the proliferation of regenerated connective tissue or to provide direct drug delivery and mechanical support. GTR/GBR membranes are highly flexible, based on a variety of polymers and polymeric nanocomposites, and can be prepared by using different methods such as, solidification-assisted compression[5], solvent casting and evaporation[6], electrospinning/electrospraying[7], coprecipitation/dynamic filtration/freeze-drying[8], thermally induced phase separation[9], among others.

Poly(ε-caprolactone) (PCL)-based electrospun scaffolds have been considered as good matrices for bone regeneration in GTR/GBR membranes due to the ability of the fibrous membrane to populate bone marrow-derived mesenchymal cells and to mediate their differentiation into osteoblastic cells.[10] PCL is a semicrystalline, bioresorbable aliphatic polyester which owes its biodegradability to the susceptibility of its ester groups to hydrolysis and the metabolization of the degradation products. Compared with poly(lactic acid), PCL degradation does not produce a local acidic environment and occurs very slowly.

The combination of a polymer with bioceramic components is a strategy inspired in

the hybrid nature of bone: a complex composite made up mostly of organic collagen fibers and hydroxyapatite, a bioactive inorganic calcium phosphate. In recent years, the incorporation of nano-hydroxyapatite (nHAp) into polymer-based scaffolds has demonstrated great potential toward the development of new bioactive membranes.[11] The interest in nHAp as inorganic nanofiller lays in its high surface area to volume ratio, high surface activity, biocompatibility, and ability to absorb a number of bioactive species.[12] The effect of hydroxyapatite/polymer composites in the biological functions of bone cells has been investigated in many in vitro studies.[7,11,13] In addition, osteoinductivity and osteoconductivity are other valuable features for its potential functionality as drug delivery carrier.[14]

Antibiotic loaded GTR/GBR membranes have demonstrated high effectiveness as antimicrobial barriers for controlled delivery systems.[15] Tetracycline (TR) and amoxicillin (AMX) were found to be the most commonly prescribed antibiotics against most periodontal pathogens.[15, 16] Incorporation of TR or AMX in GTR/GBR membranes showed to reduce the attachment *S mutans* and *A actinomycetemcomitans* to periodontal ligament cells onto the membranes.[17, 18] Ease of incorporating therapeutic agents into electrospun fibers have led to the development electrospun antimicrobial nanofibers for many biomedical applications.[19,20] Incorporation of AMX in PCL-based nanofibers obtained by electrospinning could produce third-generation membranes[21] with the ability to reduce bacterial contamination of periodontal defects and regenerative endodontics.

The aim of this study was to prepare new fibrous PCL nanocomposites via electrospinning by varying the nHAp and AMX contents incorporated in the membrane, in order to evaluate the scaffolds prospective for dental applications. The influence of the amount of nHAp on the interaction with amoxicillin, and the drug release behavior

from this nanocomposite nanofibrous membranes, were investigated. Membranes were characterized in terms of morphology, surface hydrophilicity, thermal and mechanical properties, antibiotic encapsulation efficiency and release behavior against four bacterial strains.

MATERIALS AND METHODS

Materials

PCL (Mn = 80000 g mol^{-1}) was acquired from Aldrich Chemical Co. (St Louis, MO, USA). Diammonium hydrogen phosphate was purchased from Sigma-Aldrich (Germany). Darvan 821A were purchased from R. T. Vanderbilt, USA. Amoxicillin trihydrate (AMX) was supplied by Antibiotice SA Iaşi, Romania. Deionized water was used in all experiments. All commercial materials were used without further purification. *Staphylococcus aureus* (ATCC 6538P), *Salmonella typhimurium* (ATCC 14028) were purchased from American Type Culture Collection (ATCC). *Micrococcus luteus (lizodeikticus)* and *Staphylococcus aureus* (collection strain) were obtained from the Department of Microbiology of University of Agricultural Sciences and Veterinary Medicine Cluj-Napoca and were maintained on solid agar medium at 4 °C.

Synthesis and characterization of nano-hydroxyapatite (nHAp)

nHAp was synthesized by a wet chemical method using calcium nitrate and ammonium hydrogen phosphate as Ca and P precursors. Calcium nitrate was mixed with ammonium hydrogen phosphate at ratio of Ca/P 1.67, in accordance with the standard stoichiometry for pure HAp. Two solutions of 1000 ml were prepared by dissolving separately calcium nitrate and ammonium hydrogen phosphate in deionized

water by vigorous stirring in aqueous solution at room temperature. Darvan 821A was added to both solutions as dispersing agent. pH of each aqueous solution was adjusted to 11 by using NH_4OH solution 25%. The reaction that took place is shown below:

$$10Ca(NO_3)_2 + 6(NH_4)_2HPO_4 + 8NH_4OH \rightarrow Ca_{10}(PO_4)_6(OH)_2 + 20NH_4NO_3 + 6H_2O$$

$(NH_4)_2HPO_4$ solution was dropwisely added into $Ca(NO_3)_2$ solution at 70 °C with vigorous stirring, and pH = 11 was maintained by using NH_4OH solution 25%. The suspension was kept under stirring for 12 h and then filtrated and washed three times with distilled water and anhydrous ethanol. Finally, the sample was lyophilized and thermally treated in a furnace at 300 °C for 6 h to obtain a fine dried powder.

The phase composition and crystallinity of calcined nHAp were analyzed by X-ray diffraction (XRD), with a DRON-3 diffractometer, in Bragg-Brentano geometry. The crystallite size was estimated with the Scherrer formula.[22]

Transmission electron microscopy (TEM) (H-7650 120 kV automatic microscope, Hitachi, Japan) was used to study and determine the size and morphology of nHAp.

Preparation of electrospun membranes

Preparation of the drug/ceramic/polymer solution was carried out in a one-pot procedure. AMX was dissolved in a solvent mixture of chloroform/methanol (3:1) and stirred for 12 h. Then, nHAp nanoparticles were added and the mixture was sonicated for 30 min. Finally, PCL (15% wt/v) was added to the nanohybrid AMX/nHAp dispersion and stirred for 12 h with a magnetic bar. Membranes with 0, 1 and 1.5 wt.% of AMX and 0, 10, 15 and 20 wt.% of nHAp were prepared by considering weight percentages related to PCL mass. Thomas et al. studied electrospun bioactive

nanocomposite scaffolds and reported that nHAp can be well dispersed in PCL up to the addition of 20 wt%, after ultrasonication.[11] Samples were coded as A(wt.% AMX)-H(wt.% nHAp). The mixtures were electrospun using 15-25 kV and a flow rate of 5-6 ml h^{-1}. Fibers were collected in an aluminum foil located 12 cm away from the needle tip. Membranes were exhaustively dried under vacuum for 48 h.

Membrane characterization

Morphology of the electropun membranes was examined by scanning electron microscopy (SEM, JEOL JSM6460 LV, Peabody, MA, USA) at 15 kV after gold sputtering. The mean diameter and diameter distributions were obtained by using Image ProPlus software.

Thermal properties were determined by thermogravimetric analysis (TGA) and differential scanning calorimetry (DSC). TGA were performed on a TGA-DTGA Shimadzu 50 thermal analyzer from ambient temperature to 600°C at 10°C min^{-1} under nitrogen atmosphere. DSC thermograms were obtained in a Perkin-Elmer Pyris 1 calorimeter (PerkinElmer Inc., Waltham, MA, USA). Scans were carried out from 0 to 250°C at a hearing rate of 10°C min^{-1} under nitrogen atmosphere. Crystallinity (X_c) was calculated with respect to 100% crystalline PCL (melting enthalpy = 148.05 J g^{-1}).[23] Glass transition temperature was determined in the onset of the transition.

Contact angle measurements were performed with distilled water using a ramé-hart goniometer. Attenuated total reflectance-Fourier transform infrared spectra (FTIR-ATR) were obtained using a Mattson Genesis II in the range from 600 to 4000 cm^{-1}.

XRD patterns were obtained on a Philips PW 1710 diffractometer (45 kV and 30 mA) at 2° min^{-1}, with a Cu Kα radiation (λ = 1.54 Å).

Mechanical behavior was evaluated by tensile testing from rectangular strips with an

effective length of 24.75 mm and 8 mm width. A traverse speed of 10 mm min^{-1} and a 500 N load cell were used. Membranes were tested in dried conditions and also after immersion in simulated body fluid (SBF) during 12 h, in order to mimic the environmental conditions of usage as much as possible. Data of mechanical performance in wet conditions is very important and rarely reported in literature. Samples were tested in triplicate. Elastic moduli were estimated from the linear initial part of the stress-strain curves. The yield point is defined as the point of maximum stress before irreversible deformation takes place. For comparison purposes, the end of linearity was estimated as the intersection point between the linear part and the tangent line to the curve after yield regime. The stress value at this point was registered.

Encapsulation efficiency and *in vitro* drug release measurements

In order to quantify the AMX total content, scaffolds were dissolved in the former solvent mixture and nHAp was separated by ultracentrifugation. UV-visible spectra (UV-vis) were recorded from the resulting solutions. Quantification was done by considering the peak area at λ = 227 nm. AMX content was determined with a calibration curve and the encapsulation efficiency was calculated as the percentage ratio of the loaded AMX and the initial drug in the polymeric solution.

In vitro release of AMX from the electrospun membranes was investigated by measuring the concentration of released AMX in simulated body fluid (SBF). Membrane discs (56 mg) were placed in polystyrene sterile flasks and immersed in 6 ml of SBF for 6 h, 1, 3, 7, 4, 7, 10, 15 and 20 days at 37 °C. Aliquots were taken with a 1 ml micropipette and AMX quantification was performed in a UV-Vis spectrometer (UNICAM UV-4) equipped with photomultiplier detector, using the absorbance peak at λ = 227 nm. A similar volume of fresh SBF was restored after each extraction. The

cumulative release of AMX was calculated based on a standard AMX absorbance concentration calibration curve using 0, 1.87, 3.7, 7.5, 15, 20 and 40 mg ml^{-1} as standards. The results are the average of three samples.

Microbiological evaluation of antibacterial activity of membranes

Disk diffusion tests were used to examine the antibacterial effect of AMX-loaded membranes. For this purpose, the surface of solid glucose agar in Petri dishes was inoculated with 1 ml of suspension of different four bacterial pure cultures: *Staphylococcus aureus* (ATCC 6538P), *Staphylococcus aureus* (collection strain), *Salmonella typhimurium* (ATCC 14028) and *Micrococcus luteus* formerly known as *lizodeikticus*, at a fixed density (0.5 McFarland Standard, BioMérieux, Basingstoke, UK). Then, the suspension was spread for uniformity over the entire surface of the plate using the Drigalski spatula. The excess fluid was removed, after which the plates were placed in the incubator (with the lid half-opened) in order to allow the drying of the agar surface (20 min at 37°C). Membrane discs (4 mm in diameter, 0.2 mm in thickness) containing various concentrations of AMX and nHAp (A1-H0, A1-H10, A1-H15, A1-H20, A1.5-H0, A1.5-H10, A1.5-H15 and A1.5-H20) were placed on the bacteria-inoculated agar plates, following a radial pattern, and the standard disc A0-H20 (without AMX) was placed in the center. Bacterial inhibition zone size was measured (mm) after incubation at 37°C for 24h. For each AMX concentration, three plates were inoculated with the same bacterial strain.

Data were statistically analyzed by one-way analysis of variance (ANOVA) and by Tukey's test with the level of significance set at 0.05 in order to determine the significant differences between the mean values of the tested materials.

Bioactivity testing

In vitro bioactivity of membranes was assessed by their *in vitro* apatite-forming ability on the surface of membranes during storage in SBF solution.[24] A0-H20 and A1.5-H20 samples (8 mm in diameter) were immersed in 15 ml of SBF and stored at 37 °C for 21 days. SBF solution were prepared according to Kokubo's SBF solution[24] using the standard ion composition (Na^+ 142.0 mM, K^+ 5.0 mM, Mg^{2+} 1.5 mM, Ca^{2+} 2.5 mM, Cl^- 147.8 mM, HCO_3^- 4.2 mM, HPO_4^{2-} 1.0 mM, and SO_4^{2-} 0.5 mM), buffered at the physiological pH of 7.40 at 37 °C, with tris(hydroxymethyl)amino methane and hydrochloric acid. After 21 days, samples were removed from the SBF solution, washed with distilled water, and stored in a desiccator prior to SEM/EDX analysis. A1-H20 and A1.5-H20 samples were mounted on stubs and gold sputter-coated (Bio-Rad Polaron Division SEM Coating System, Polaron Instruments Inc., Agawan, MN, USA).

RESULTS AND DISCUSSION

Characterization of nHAp

Figure 1 illustrates the XRD pattern of the synthesized calcined nHAp. X-ray diffraction revealed nHAp in a crystalline form (JCPDS card No.09-0432) with a mean crystallite size of 57.9 nm. Crystals of nHAp rods particles with 11 – 21 nm in diameter and 20–66 nm in length were detected (Figure 2).

Characterization of electrospun nanocomposite membranes

Fiber size and morphology of electrospun fibers depend on a number of factors, including intrinsic solution properties, processing and environmental parameters.[2] The spinning conditions used in this work were selected after screening experiments that led to the production of uniform, bead-free, continuous fibers. SEM analysis revealed a

typical electrospun structure of randomly oriented bead-free fibers, with highly anisotropic fiber distribution, interconnected open macropores, and pore distribution throughout the structure (Figure 3a). Fiber diameter frequency distribution is shown in Figure 3b, the mean fiber diameters being in the range of 1.2 to 2.2 µm.

TGA thermograms corresponding to PCL, AMX, nHAp and A1.5 membrane series are shown in Figure 4. As expected, the residual mass is in agreement with nHAp contents in the membranes. However, the detection of the ceramic particles in the surface by XRD and ATR-FTIR did not show the same trend when AMX is present in the membranes. Indeed, the nHAp-related diffraction (Figure 5) and infrared peaks (Figure 6) did not follow an intensity trend that matches the nHAp contents in the membranes containing AMX. Given that membranes without AMX indeed follow the expected trend, as observed by FTIR, the incorporation of the antibiotic seems to alter the distribution of nHAp within the fibers. Thus, when membranes were prepared with AMX, nHAp particles were distributed not only in the surface but also within the fibers.

Table 1 shows a slight increase in the surface hydrophilicity for the drug-loaded membranes with respect to pristine PCL, though no clear trend was observed among the different compositions. DSC thermograms of nanocomposite membranes revealed that PCL melting temperature and crystallinity degree have no significant variations with the incorporation of AMX and nHAp, as seen in Table 1. The absence of appreciable changes in melting enthalpy and crystallinity with the addition of nHAp in neat PCL nanofibers was also previously reported.[11]

Mechanical properties of antibiotic-loaded membranes were tested before and after immersion in SBF, in order to mimic the environmental conditions. Stress-strain curves, elastic modulus and apparent yield stress for A1.5 series in both conditions are shown in Figure 7 (a-c). The dried membrane with no ceramic nanofiller (A1.5-H0) showed a

large elastic range and relatively high elastic modulus. It is known that the interface adhesion of polymer matrix and nanofillers plays a key role among other factors affecting the properties of nanocomposites. The incorporation of nHAp produced a plasticization effect resulting in a larger plastic deformation (~ 400 % with 10% nHAp). Similarly, a study on electrospun PCL/nano$CaCO_3$ membranes showed a comparable behavior for the composite containing 10% of this inorganic filler content.[25] However, Thomas *et al.*[11] reported an opposite trend in PCL/nHAp-based nanocomposites without AMX. They found that an increase in nHAp content led to an increase in both tensile strength and tensile modulus, because of a good interface bonding of the polymer matrix and nHAp filler particles. In our system, it appeared that the strong interaction of nHAp with AMX decreases the interface adhesion with the PCL matrix, leading to a decrease in tensile modulus and ultimate strength.

In comparison, the series tested after SBF immersion showed a significant decrease of the elastic modulus for A1.5-H0 but a moderate effect for the remaining membranes. This could be explained by the fact that the plasticization effect of water is more evident for membranes with no filler. Besides this particular case, the elastic moduli did not show significant differences. In both conditions, the post-yield regime changed completely because of the nHAp incorporation, as evidenced by the decreased stress yield values and the higher permanent deformations encountered.

AMX release from nanocomposite membranes

Local controlled delivery of drugs is preferred to systemic administration due to the improved drug effectiveness, selective targeting, decreased side effects, and reduced frequency of administration. Therefore, it is of utmost importance to investigate and to modulate the release profiles for the specific applications. The cumulative release

profiles of AMX from the prepared membranes, displayed in Figure 8, present two stages: a first rapid release or burst effect, followed by a slow and prolonged second stage. The initial burst, found in many controlled drug delivery systems, has been explained by a number of mechanisms, including surface desorption, pore diffusion, or the lack of a diffusion front barrier regulating the diffusive process.[26] For the delivery of antibiotic drugs, an initial burst is actually ideal since it is important to eliminate the intruding bacteria immediately after the dental surgical intervention, preventing their proliferation.[27] However, a continued release of antibiotic is required to prevent further population of residual organisms for the prevention of bacterial growth and colonization.

The fraction of AMX released after 1 day depended on the nHAp content. Therefore, an increase in nHAp content in A1 or A1.5 series led to a decrease in the burst effect. Amoxicillin contains several polar groups (-NH, -OH) which are able to establish chemical bonding by hydrogen-bonding forces with hydroxyl groups of hydroxyapatite particles. These interactions lead to the formation of a nanohybrid AMX-nHAP. Besides the lower extent of the interactions of PCL with AMX and nHAP, the aliphatic polyester is still a suitable matrix for the PCL/AMX/nHAp system.

A1-H20 and A1.5-H20 membranes exhibited the lowest amount of AMX release after 1 day (40 and 38%, respectively). On the other hand, the complete release of AMX from membranes without nHAp (A1-H0 and A1.5-H0) occurred in only 7 days, whereas for 10 wt.% nHAp the total content was released in 21 days, and it was not yet completed for 15 wt.% nHAp (91-93%) and 20 wt.% nHAp (84-85%) in the same period. These results are in agreement with the presence of physical interactions, which modulate the release behavior.

Zheng *et al.*[28] reported the separate preparation of AMX-loaded nHAp nanohybrids,

that were blended with a polymer solution in a second stage, prior to electrospinning. From the resulting PLGA based nanofibers, a release of 16% was found after the first day, but only 35% of AMX was released after 18 days. The strong interaction between AMX and nHAp could be responsible for the decrease in burst release, but at the same time the cause of the incomplete AMX delivery. The subsequent mineralization could completely block the antibiotic release. In other different system, Valarezo *et al.*[29] studied PCL-based membranes with AMX intercalated in layered double hydroxide (LDH) nanoparticles. The authors found a burst release of about 45% in the first day and fractions in the range of 70 to 100% for AMX/LDH contents from 3 to 7 wt.%. These results for the intercalated AMX/clay are in close agreement with our observations for AMX/nHAp.

Table 2 shows the decrease in encapsulation efficiency of AMX with increasing nHAp content in both A1 and A1.5 series. Again, this result can be mainly attributed to the interactions between AMX and nHAp. A fraction of AMX remained adsorbed on the nHAp surface after membrane dissolution and ultracentrifugation processes, decreasing the drug availability.

Microbiological evaluation of antibacterial activity of membranes

The studied bacterial strains from the genera *Staphylococcus* (gram-positive coccal bacterium), *Micrococcus* (gram-positive cocci) and *Salmonella* (gram-negative bacteria), were selected because of their proven *in vitro* susceptibility to AMX. *Staphylococci* are commensally of the skin, skin glands, and mucous membranes, both in humans and in animals, that show their pathogenic ability through virulence and a wide range of aggression and toxic factors.[30] *S. aureus* (gram-positive coccal bacterium) is often involved in the production of several types of diseases of the oral cavity:

stomatitis, orofacial granulomas[31], periodontitis[32-35], peri-implant mucositis[36], endodontic infections[37] and even tooth decay.[38,39] *Micrococcus luteus* (gram positive cocci) is considered a non-pathogenic germ usually isolated from the external environment (dust, soil, air, different objects), but it can be frequently found onto the skin, mucous membranes of the nasal cavities and in the oral cavity.[40, 41] Finally, *Salmonella typhimurium* is one of the most prevalent serovars, predominantly as a gastrointestinal tract pathogen and could be found the oral cavity.[42] *Salmonella typhimurium* was tested for evaluation of mutagenic capacity of some dental materials.[43]

The antibacterial activity of neat membrane (A0b20) and AMX-loaded membranes (A1 and A1.5 series) are presented in Table 2 and Figure S1 (please see Supporting Information). As expected, membranes with 1.5 wt.% AMX showed higher antimicrobial activity than those with 1 wt.% AMX. This observation, in agreement with other studies[28], is related with the quantity of incorporated AMX. A0-H20 membrane based on PCL and nHAp was used as negative control. The material did not display bacterial inhibition area and confirmed that the membranes antimicrobial activity is due to the AMX release. There were slight differences between strains of *Micrococcus luteus*, *Staphylococcus aureus* (ATCC 6538P) and *Staphylococcus aureus* (collection strain). The lowest antimicrobial activity was observed for *Staphylococcus aureus* (collection strain). Membranes without nHAp (A1-H0 and A1.5-H0) showed higher bacterial inhibition area than their counterparts containing inorganic filler. This faster AMX release could be due to higher water sorption in the matrices without inorganic filler. Absorbed water can diffuse inside of PCL matrix and it can act as AMX carrier from inside of polymer composite, spreading around of samples by agar diffusion. The lower AMX release with increasing nHAp content is well correlated with the observed antimicrobial results (Table 2 and Figure S1).

Bioactivity of nanocomposite membranes

SEM micrographs of membrane surface after 21 days storage in SBF are presented in Figure 9a for A1-H20 membrane, and in Figure 9c-e for A1.5-H20 membrane. As it can be clearly seen, the nanofibers surface show the formation of new apatite crystals (Figure 9a-e red double arrows) and microporosities (Figure 9a,d,e yellow arrows) probably associated with PCL degradation around nHAp/AMX particles and/or with solubility/leaching of nHAp/AMX particles during storage. nHAp on the fiber surface was exposed continuously to SBF and induced apatite nucleation and crystallization. Moreover, solubility of nHAp surface particles and release of Ca^{+2} and HPO_4^{2-} ions in SBF induced ion saturation in the solution. EDX analysis for A1-H20 (Figure 9b) and A1.5-H20 (Figure 9f) showed the presence of calcium, phosphorous and chlorine at the surface, thus confirming the formation of new apatite crystals with ratio Ca/P=1.55. Although the Ca/P ratio in pure hydroxyapatite is 1.67, the formation of calcium-deficient apatite at Ca/P ratio is in agreement with other studies reporting Ca/P values such as 1.06, 1.27, 1.55 or 1.6.[44-49] The chlorine ions detected at the membrane surface may be due to some infiltration from the SBF solution, and could be found in the structure of apatite layer as chlorapatite $Ca_{10}(PO_4)_6(Cl)_2$.[44-46]

CONCLUSIONS

A series of electropun nanocomposite fibrous membranes was obtained by varying the concentration of antibiotic (0, 1 and 1.5 wt.%) and nHAp (0-20 wt.%) incorporated in the composition. Uniform bead-free microfibrous non-woven mats were obtained in all cases. The incorporation of AMX seemed to modify the nHAp distribution within the matrix. Moreover, the interaction between AMX and nHAp affected the mechanical

performance before and after SBF immersion, and modulated the AMX release profiles. *In vitro* release curves presented an initial high-rate antibiotic release stage, which is advantageous for GTR/GBR therapy, followed by a sustained release of 85-100% of the total drug content during 3 weeks.

The antimicrobial activity of the AMX-loaded membranes depended on both AMX and nHAp contents. Membranes with the highest AMX content (A1.5 series) are more efficient in terms of antimicrobial activity and lead to a reduction in the burst effect. Membranes with the highest nHAp content exhibited a pronounced bioactivity after 21 days immersion in SBF, as assessed by their ability to form apatite on their surfaces. However, a choice of the optimal amount of nHAp implies not only a good biomineralization (highest quantity) but also a compromise between the encapsulation efficiency and the inhibition effect. Among the studied parameters, an intermediate filler content (H10 or H15) would generate a smooth release profile without hindering the AMX delivery efficiency. Biomineralization of membrane surface after SBF storage could have a beneficial effect *in vivo* and confirms the possibility of new bone formation at the surface and inside of membrane pores after surgery.

The prepared electrospun nanocomposite amoxicillin-loaded mats could be promising third-generation GTR/GBR membranes for dental and tissue engineering applications.

ACKNOWLEDGEMENTS

The authors acknowledge COST Action MP1206, Argentinean Agency for Scientific and Technological Promotion (PICT 224), CONICET (PIP 089) and the Romanian National Authority for Scientific Research, CNCS-UEFISCDI project 127/2014, for financial support. The authors would also like to thank the collaboration of Dr. Roxana Trusca from METAV Research & Development, Bucharest, Romania for her assistance

in SEM micrographs of membranes after SBF storage and Dr. Katona Gabriel (Babeş-Bolyai University, Cluj-Napoca, Romania) for TEM investigation.

REFERENCES

1. Agarwal S, Greiner A, Wendorff JH. Functional materials by electrospinning of polymers. Progr Polym Sci 2013;38:963-991.
2. Li H, Xu Y, Xu H, Chang J. Electrospun membranes: control of the structure and structure related applications in tissue regeneration and drug delivery. J Mater Chem B 2014;2:5492-5510.
3. Zamani M, Prabhakaran MP, Ramakrishna S. Advances in drug delivery via electrospun and electrosprayed nanomaterials. Int J Nanomedicine 2013;8:2997-3017.
4. He C, Nie W, Feng W. Engineering of biomimetic nanofibrous matrices of drug delivery and tissue engineering. J Mater Chem B 2014;2:7828-7848.
5. Sun F, Kang HG, Ryu SC, Kim JE, Park EY, Hwang DY, Lee J. Guided bone regeneration using a flexible hydroxyapatite patch. J Biomed Nanotechnol 2013;9:1914-1920.
6. Zeng S, Fu S, Guo G, Liang H, Qian Z, Tang X, Luo F. Preparation and characterization of nano-hydroxyapatite/poly(vinyl alcohol) composite membranes for guided bone regeneration. J Biomed Nanotechnol 2011;7:549-557.
7. Ribeiro N, Sousa SR, van Blitterswijk CA, Moroni L, Monteiro FJ. A biocomposite of collagen nanofibers and nanohydroxyapatite for bone regeneration. Biofabrication 2014;6:035015.
8. Teng SH, Lee EJ, Yoon BH, Shin DS, Kim HE, Oh JS. Chitosan/nanohydroxyapatite composite membranes via dynamic filtration for guided bone regeneration. J Biomed Mater Res A 2009;88:569-580.

9. Wei G, Ma PX. Structure and properties of nano-hydroxyapatite/polymer composite scaffolds for bone tissue engineering. Biomaterials 2004;25:4749-4757.

10. Yoshimoto H, Shin YM, Terai H, Vacanti JP. A biodegradable nanofiber scaffold by electrospinning and its potential for bone tissue engineering. Biomaterials 2003;24:2077-2082.

11. Thomas V, Jagani S, Johnson K, Jose MV, Dean DR, Vohra YK, Nyairo E. Electrospun bioactive nanocomposite scaffolds of polycaprolactone and nanohydroxyapatite for bone tissue engineering. J Nanosci Nanotechnol 2006;6:487-493.

12. Zhang J, Wang Q, Wang A. In situ generation of sodium alginate/hydroxyapatite nanocomposite beads as drug-controlled release matrices. Acta Biomater 2010;6:445-454.

13. Yu HS, Jang JH, Kim TI, Lee HH, Kim HW. Apatite-mineralized polycaprolactone nanofibrous web as a bone tissue regeneration substrate. J Biomed Mater Res A 2009;88:747-754.

14. Kim HW, Knowles JC, Kim HE. Hydroxyapatite/poly(epsilon-caprolactone) composite coatings on hydroxyapatite porous bone scaffold for drug delivery. Biomaterials 2004;25:1279-1287.

15. Markman C, Fracalanzza SE, Novaes ABJ, Novaes AB. Slow release of tetracycline hydrochloride from a cellulose membrane used in guided tissue regeneration. J Periodontol 1995;66:978-983.

16. Ahmad N, Saad N. Effects of antibiotics on dental implants: a review. J Clin Med Res 2012;4:1-6.

17. Hung SL, Lin YW, Chen YT, Ling LJ. Attachment of periodontal ligament cells onto various antibiotics-loaded guided tissue regeneration membranes. Int J

Periodontics Restorative Dent 2005;25:265-275.

18. Cheng CF, Wu KM, Chen YT, Hung SL. Bacterial adhesion to antibiotic-loaded guided tissue regeneration membranes - a scanning electron microscopy study. J Formos Med Assoc 2015;114:35-45.

19. Albuquerque MT, Valera MC, Moreira CS, Bresciani E, de Melo RM, Bottino MC. Effects of ciprofloxacin-containing scaffolds on enterococcus faecalis biofilms. J Endod 2015;41:710-714.

20. Abrigo M, McArthur SL, Kingshott P. Electrospun nanofibers as dressings for chronic wound care: advances, challenges, and future prospects. Macromol Biosci 2014;14:772-792.

21. Sam G, Pillai BR. Evolution of Barrier Membranes in Periodontal Regeneration- "Are the third Generation Membranes really here?" J Clin Diagn Res 2014;8:14-17.

22. Klug HP, Alexander LE. X-ray Diffraction Procedures. New York: Wiley; 1954.

23. Van Krevelen DW. Properties of polymers, 3rd ed. Amsterdam: Elsevier; 1990:121.

24. Kokubo T, Takadama H. How useful is SBF in predicting in vivo bone bioactivity? Biomaterials 2006;27:2907-2915.

25. Fujihara K, Kotaki M, Ramakrishna S. Guided bone regeneration membrane made of polycaprolactone/calcium carbonate composite nano-fibers. Biomaterials 2005;26:4139-4147.

26. Sill TJ, von Recum HA. Electrospinning: applications in drug delivery and tissue engineering. Biomaterials 2008;29:1989-2006.

27. Huang X, Brazel CS. On the importance and mechanisms of burst release in matrix-controlled drug delivery systems. J Control Release 2001;73:121-136.

28. Zheng F, Wang S, Wen S, Shen M, Zhu M, Shi X. Characterization and antibacterial activity of amoxicillin-loaded electrospun nano-

hydroxyapatite/poly(lactic-co-glycolic acid) composite nanofibers. Biomaterials 2013;34:1402-1412.

29. Valarezo E, Tammaro L, Gonzalez S, Malagón O, Vittoria V. Fabrication and sustained release properties of poly(ε-caprolactone) electrospun fibers loaded with layered double hydroxide nanoparticles intercalated with amoxicillin. Appl Clay Sci 2013;72:104–109.

30. Vadyvaloo V, Otto M. Molecular genetics of Staphylococcus epidermidis biofilms on indwelling medical devices. Int J Artif Organs 2005;28:1069-1078.

31. Gibson J, Wray D, Bagg J. Oral staphylococcal mucositis: A new clinical entity in orofacial granulomatosis and Crohn's disease. Oral Surg Oral Med Oral Pathol Oral Radiol Endod 2000;89:171-176.

32. Rams TE, Feik D, Slots J. Staphylococci in human periodontal diseases. Oral Microbiol Immunol 1990;5:29-32.

33. Murdoch FE, Sammons RL, Chapple IL. Isolation and characterization of subgingival staphylococci from periodontitis patients and controls. Oral Dis 2004;10:155-162.

34. Fritschi BZ, Albert-Kiszely A, Persson GR. Staphylococcus aureus and other bacteria in untreated periodontitis. J Dent Res 2008;87:589-593.

35. Petti S, Boss M, Messano GA, Protano C, Polimeni A. High salivary Staphylococcus aureus carriage rate among healthy paedodontic patients. New Microbiol 2014;37:91-96.

36. Heitz-Mayfield LJ, Lang NP. Comparative biology of chronic and aggressive periodontitis vs. peri-implantitis. Periodontology 2000. 2010;53:167-181.

37. Poeschl PW, Crepaz V, Russmueller G, Seemann R, Hirschl AM, Ewers R. Endodontic pathogens causing deep neck space infections: clinical impact of

different sampling techniques and antibiotic susceptibility. J Endod 2011;37:1201-1205.

38. Ohara-Nemoto Y, Haraga H, Kimura S, Nemoto TK. Occurrence of staphylococci in the oral cavities of healthy adults and nasal oral trafficking of the bacteria. J Med Microbiol 2008;57:95-99.

39. Kouidhi B, Zmantar T, Hentati H, Bakhrouf A. Cell surface hydrophobicity, biofilm formation, adhesives properties and molecular detection of adhesins genes in Staphylococcus aureus associated to dental caries. Microb Pathog 2010;49:14-22.

40. Micrococcus luteus. http://en.citizendium.org/wiki/Micrococcus_luteus (accessed October 18, 2015).

41. Purmal K, Chin S, Pinto J, Yin WF, Chan KG. Microbial contamination of orthodontic buccal tubes from manufacturers. Int J Mol Sci 2010;11:3349-3356.

42. Finlay BB. Interactions between Salmonella typhimurium, enteropathogenic Escherichia coli (EPEC), and host epithelial cells. Adv Dent Res 1995;9:31-36.

43. Kaplan C, Diril N, Sahin S, Cehreli MC. Mutagenic potentials of dental cements as detected by the Salmonella/microsome test. Biomaterials 2004;25:4019-4027.

44. Furtos G, Naghiu MA, Declercq H, Gorea M, Prejmerean C, Pana O, Tomoaia-Cotisel M. Nano forsterite biocomposites for medical applications: Mechanical properties and bioactivity. J Biomed Mater Res B Appl Biomater 2015 Jun 24. doi: 10.1002/jbm.b.33396.

45. Ajami E, Aguey-Zinsou KF. Calcium phosphate growth at electropolished titanium surfaces. J Funct Biomater 2012;3:327-348.

46. Oliveira AL, Malafaya PB, Reis RL. Sodium silicate gel as a precursor for the *in vitro* nucleation and growth of a bone-like apatite coating in compact and porous polymeric structures. Biomaterials 2003;24:2575-2584.

47. Vandiver J, Patel N, Bonfield W, Christine O. Nanoscale morphology of apatite precipitated onto synthetic hydroxyapatite from simulated body fluid. Key Eng Mater 2005;284/286:497-500.

48. Radin SR, Ducheyne P. The effect of calcium phosphate ceramic composition and structure on in vitro behavior. II. Precipitation. J Biomed Mater Res 1993;27:35-45.

49. Kanzaki N, Onuma K, Ito A, Teraoka K, Tateishi T, Tsutsumi S. Direct growth rate measurement of hydroxyapatite single crystal by moire phase shift. J Phys Chem B 1998;102:6471–6476.

Figure Captions:

Figure 1. X-ray diffraction pattern for the nHAp synthesized.

Figure 2. TEM image of the synthesized nHAp powder.

Figure 3. a) SEM micrographs of pristine and drug-loaded membranes. b) Fiber diameter frequency distributions.

Figure 4. Thermogravimetric curves obtained for nHAp, AMX, PCL and A1.5 nanocomposite membranes with different nHAp contents.

Figure 5. XRD diffractograms of the raw materials and A1.5 series with different nHAp contents.

Figure 6. ATR-FTIR normalized spectra of A0, A1 and A1.5 series with different nHAp contents.

Figure 7. Mechanical characterization: a) stress-strain curves, b) elastic modulus and c) yield stress for A1.5 series with different nHAp contents before and after 12 h immersion in SBF.

Figure 8. *In vitro* AMX release profiles from electrospun membranes containing different nHAP and AMX contents (1 wt.% relative to PCL: filled symbols, and 1.5 wt.%: empty symbols)

Figure 9. SEM micrographs of (a) A1-H20 and (c,d,e) A1.5-H20. EDX Analysis of (b) A1-H20 and (f) A1.5-H20. Note: red double arrows indicate new apatite crystal formed at the surface of nanofibers from membranes; yellow arrow pores inside the fibers.

Supplementary materials

Figure S1. Digital images of inhibition zones after 24 h produced by A0-H20, A1-H0, A1-H10, A1-H15, A1-H20, A1.5-H0, A1.5-H10, A1.5-H15 and A1.5-H20 membranes on: (a1-a2) *Micrococcus luteus*, (b1-b2) *Staphylococcus aureus* (ATCC 6538P), (c1-c2) *Salmonella typhimurium* (ATCC 14028), (d1-d2) *Staphylococcus aureus* (collection strain). A0-H20 was used as control without AMX.

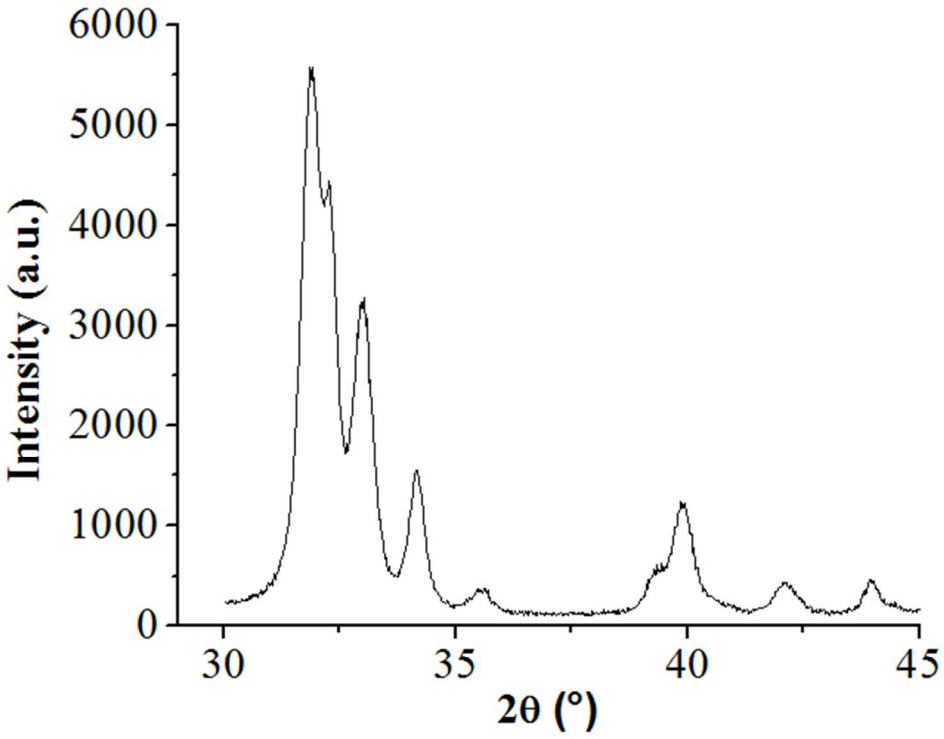

Figure 1. X-ray diffraction pattern for the nHAp synthesized.
57x45mm (300 x 300 DPI)

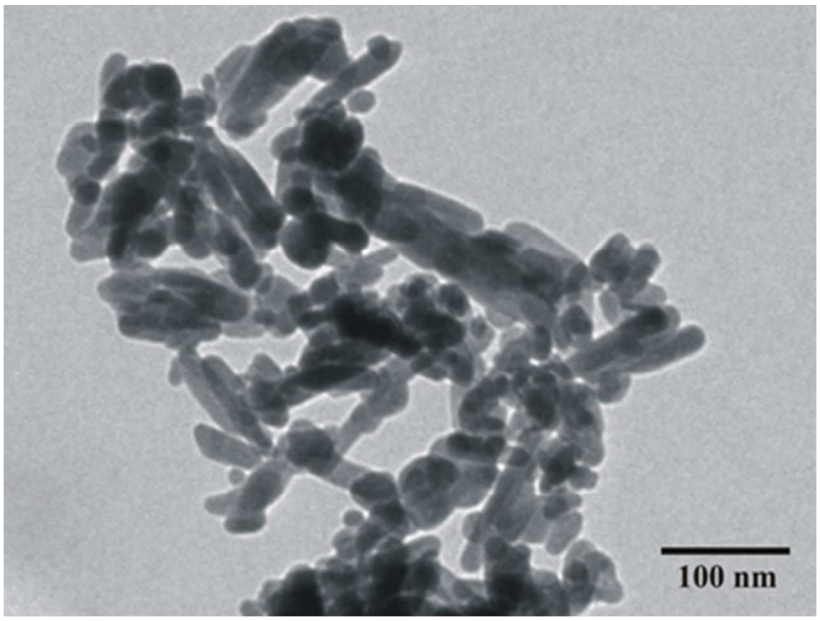

Figure 2. TEM image of the synthesized nHAp powder.
34x25mm (300 x 300 DPI)

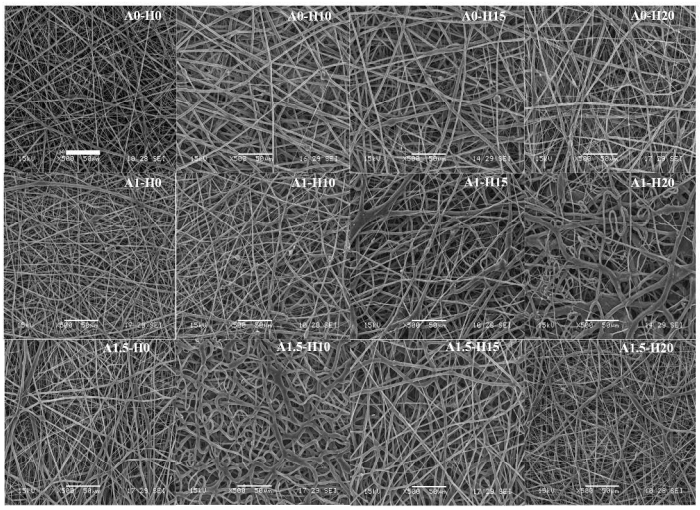

a)

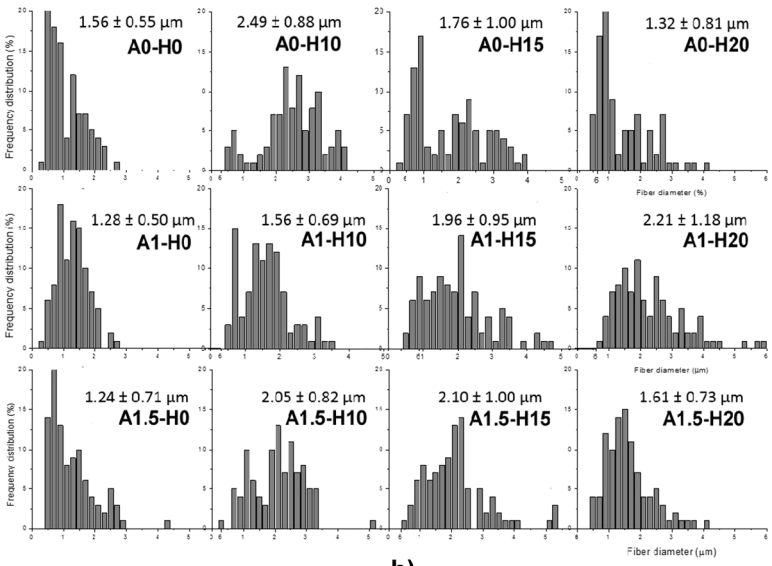

b)

Figure 3. a) SEM micrographs of pristine and drug-loaded membranes. b) Fiber diameter frequency distributions.
256x369mm (300 x 300 DPI)

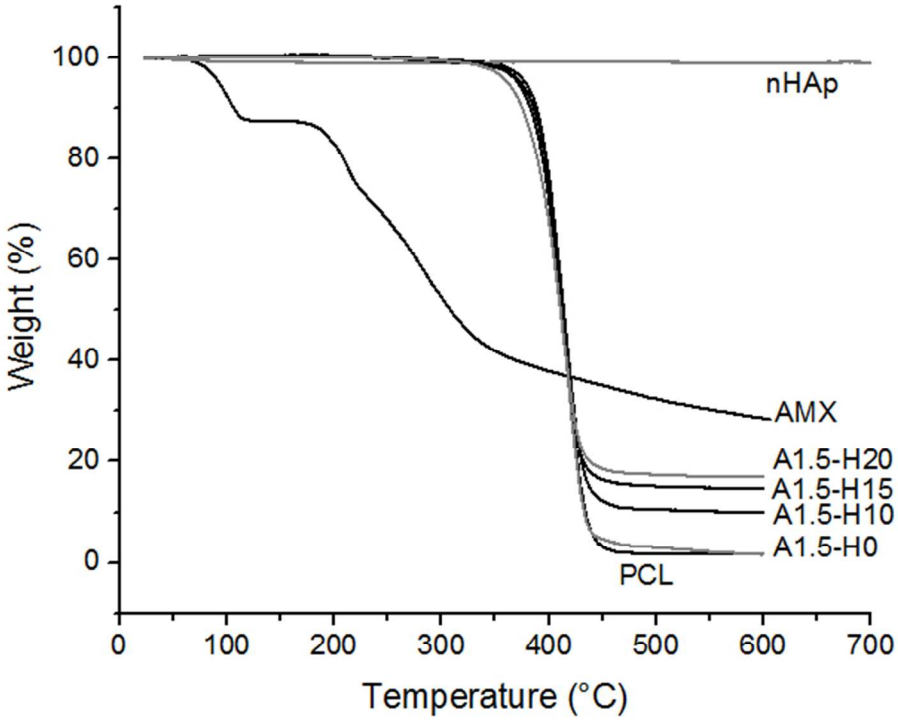

Figure 4. Thermogravimetric curves obtained for nHAp, AMX, PCL and A1.5 nanocomposite membranes with different nHAp contents.
57x44mm (300 x 300 DPI)

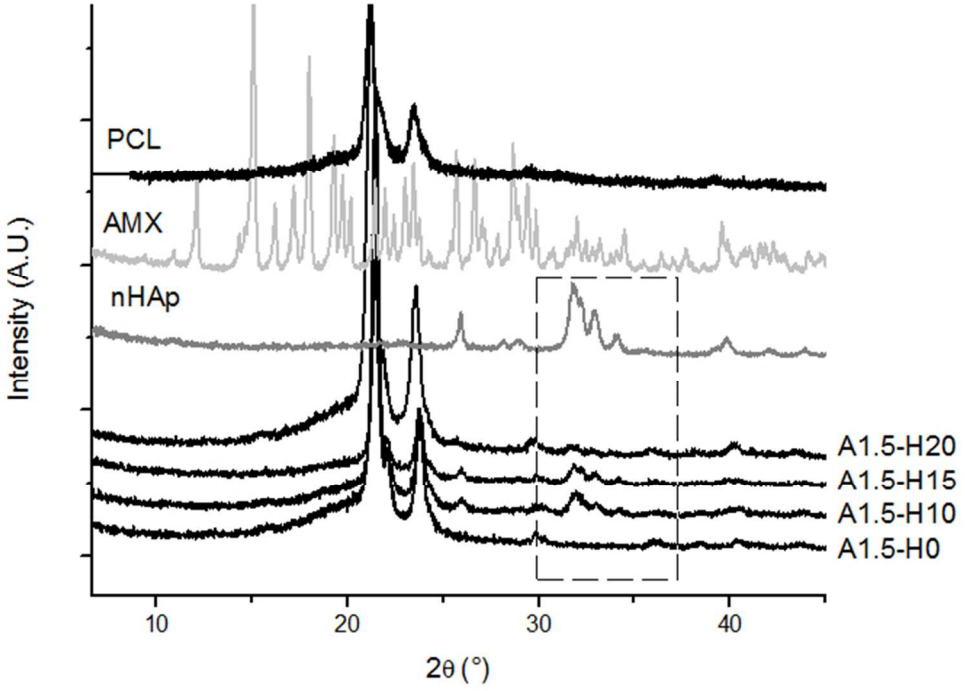

Figure 5. XRD diffractograms of the raw materials and A1.5 series with different nHAp contents.
58x42mm (300 x 300 DPI)

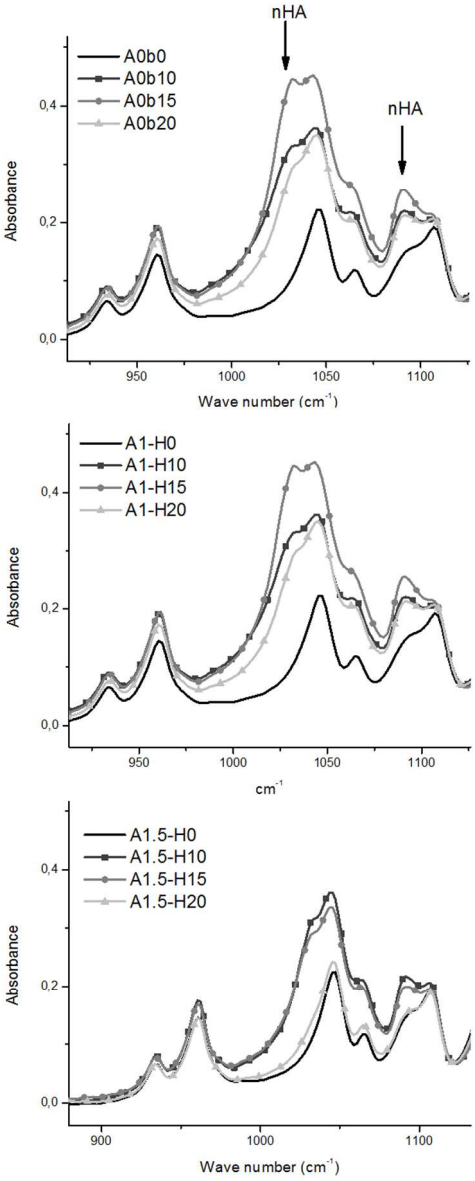

Figure 6. ATR-FTIR normalized spectra of A0, A1 and A1.5 series with different nHAp contents.
54x131mm (300 x 300 DPI)

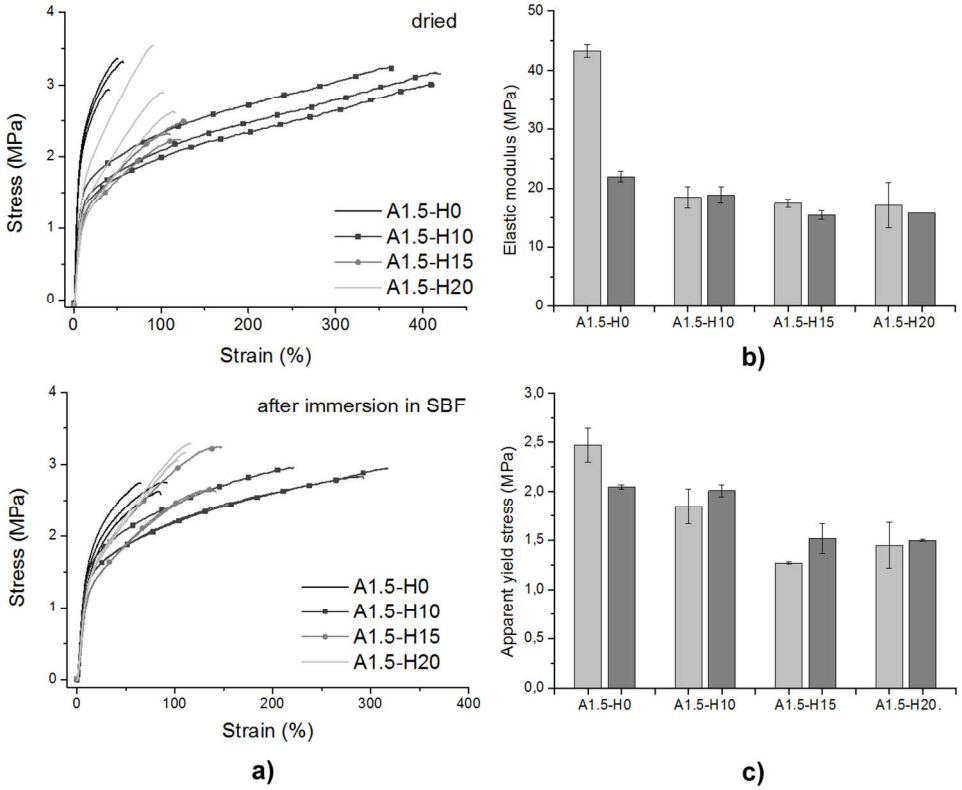

Figure 7. Mechanical characterization: a) stress-strain curves, b) elastic modulus and c) yield stress for A1.5 series with different nHAp contents before and after 12 h immersion in SBF.
120x98mm (300 x 300 DPI)

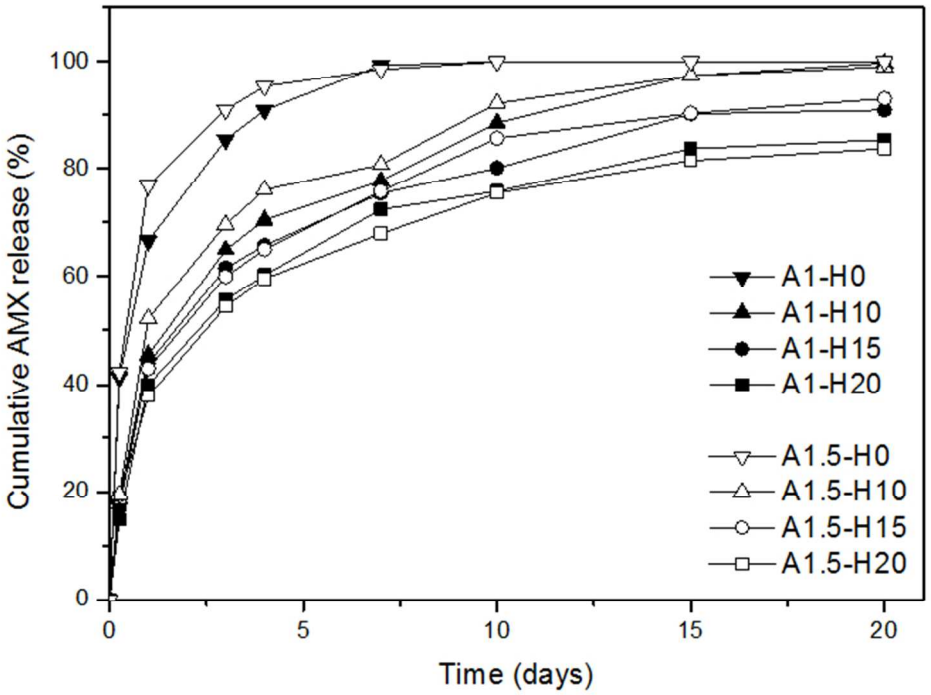

Figure 8. In vitro AMX release profiles from electrospun membranes containing different nHAP and AMX contents (1 wt.% relative to PCL: filled symbols, and 1.5 wt.%: empty symbols).
59x43mm (300 x 300 DPI)

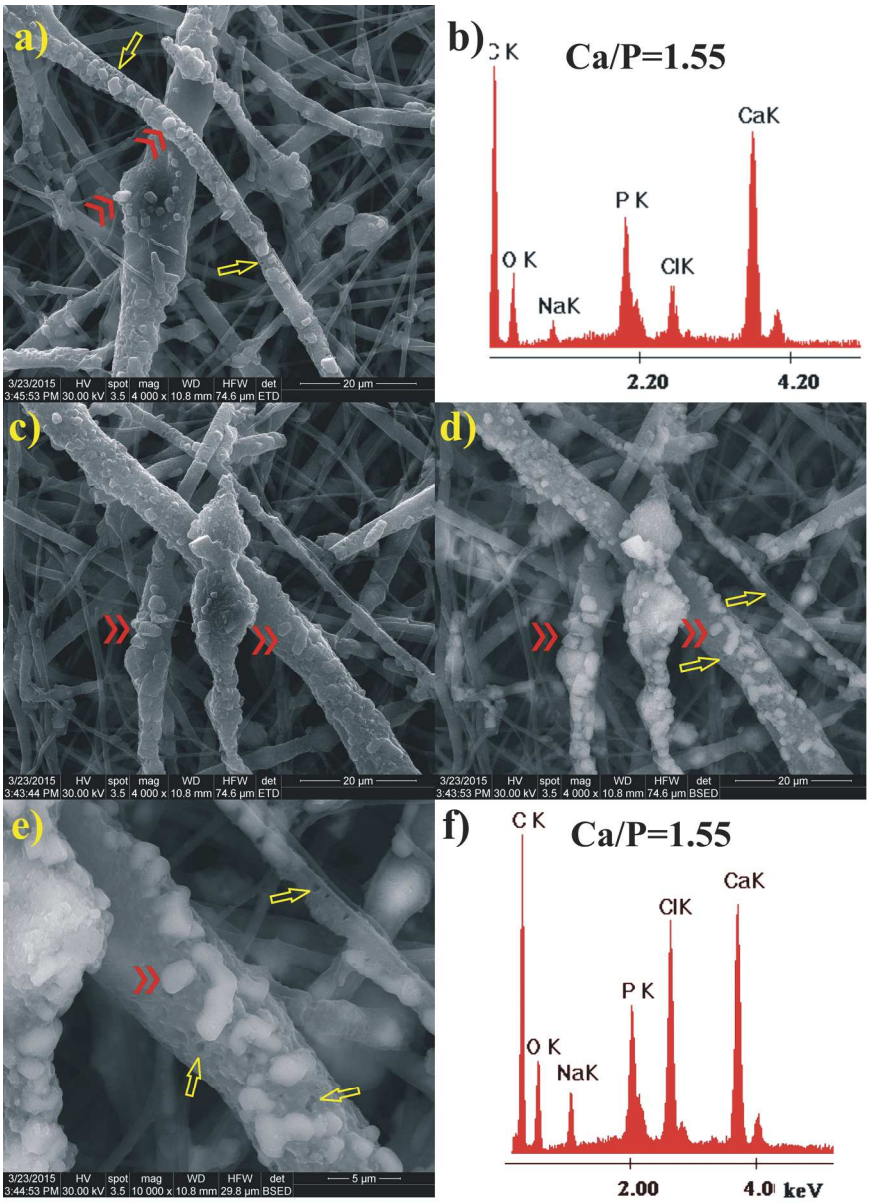

Figure 9. SEM micrographs of (a) A1-H20 and (c,d,e) A1.5-H20. EDX Analysis of (b) A1-H20 and (f) A1.5-H20. Note: red double arrows indicate new apatite crystal formed at the surface of nanofibers from membranes; yellow arrow pores inside the fibers.

Table 1. Contact angle measurements and thermal properties of nanocomposite membranes.

Sample	Contact angle (°)	T_m (ºC)	X_c (%)
A0-H0 (PCL)	126.9 ± 0.6	59.6	42.0
A0-H10	122.6 ± 0.7	58.6	38.9
A0-H15	121.6 ± 2.6	59.3	41.1
A0-H20	128.7 ± 1.2	59.0	42.2
A1-H0	121.5 ± 3.4	59.1	42.6
A1-H10	122.2 ± 5.2	58.7	40.1
A1-H15	116.8 ± 6.8	58.7	41.6
A1-H20	110.4 ± 2.5	59.0	40.8
A1.5-H0	123.2 ± 4.1	60.7	42.3
A1.5-H10	119.6 ± 2.1	57.9	40.1
A1.5-H15	124.6 ± 1.4	57.8	40.6
A1.5-H20	121.7 ± 1.9	57.7	38.9

Table 2. Encapsulation efficiency and representative inhibition zones after 24 h against: *Micrococcus luteus*; *Staphylococcus aureus* (ATCC 6538P); *Salmonella typhimurium* (ATCC 14028); *Staphylococcus aureus* (collection strain).

Sample	AMX encapsulation efficiency (%)	Mean diameter inhibition (mm) (SD)			
		Micrococcus luteus	*Staphylococcus aureus* (ATCC 6538P)	*Salmonella typhimurium* (ATCC 14028)	*S. aureus* (collection strain)
A0-H20 (control)	-	0	0	0	0
A1-H0	98.07 (8.35)	37.27 (2.61)^{a}	32.89 (1.63)^{a}	17.35 (2.88)^{a}	28.99 (0.74)^{a}
A1-H10	96.55 (6.98)	31.51 (2.56)^{b}	29.66 (1.70)^{b}	13.87 (1.07)^{a,b}	25.46 (1.81)^{a,b}
A1-H15	85.14 (11.73)	24.29 (2.89)^{b,c}	21.61 (2.34)^{c}	12.21 (3.50)^{a,b,c}	23.34 (2.94)^{b,c}
A1-H20	70.32 (8.30)	19.21 (8.60)^{c}	17.62 (2.70)^{c}	10.15 (0.66)^{b,c,d}	17.74 (1.60)^{c}
A1.5-H0	99.66 (23.71)	45.52 (1.01)^{a,d}	37.52 (1.39)^{a,d}	19.45 (0.80)^{a,e}	30.62 (0.59)^{a,b,d}
A1.5-H10	98.76 (13.61)	41.95 (0.69)^{a,d,e}	34.81 (1.86)^{a,d,e}	20.27 (1.20)^{a,e,f}	28.10 (3.93)^{a,b,c,d,e}
A1.5-H15	96.49 (7.14)	38.02 (0.76)^{a,b,d,e,f}	32.10 (1.13)^{a,b,e,f}	16.63 (1.38)^{a,b,c,e,f,g}	27.21 (0.84)^{a,b,c,d,e,f}

A1.5-H20	88.45 (3.00)	35.52 (3.57)^{a,b,d,e,f}	29.60 (0.30)^{a,b,f}	14.93 (2.62)^{a,b,c,d,e,f,g}	24.28 (0.54)^{a,b,c,f}

Note: Superscript letters $^{a\text{-}f}$ within columns indicate mean values not statistically significant different from each other, when compared using the Tukey test, $P > 0.05$